*Supporting Information*

# Hotspot identification and Drug Design of Protein-Protein Interaction Modulators using the Fragment Molecular Orbital Method

Stefania Monteleone[1], Dmitri G. Fedorov[2], Andrea Townsend-Nicholson[3], Michelle Southey[1], Michael Bodkin[1] and Alexander Heifetz[1]*

[1]Evotec UK Ltd., 114 Innovation Drive, Milton Park, Abingdon, Oxfordshire OX14 4RZ, United Kingdom

[2]NRI, National Institute of Advanced Industrial Science and Technology (AIST), 1-1-1 Umezono, Tsukuba, Ibaraki 305-8568, Japan

[3]Institute of Structural & Molecular Biology, Research Department of Structural & Molecular Biology, Division of Biosciences, University College London, London, WC1E 6BT, United Kingdom

**Corresponding Author**

Dr. Alexander Heifetz, email address: Alexander.Heifetz@evotec.com

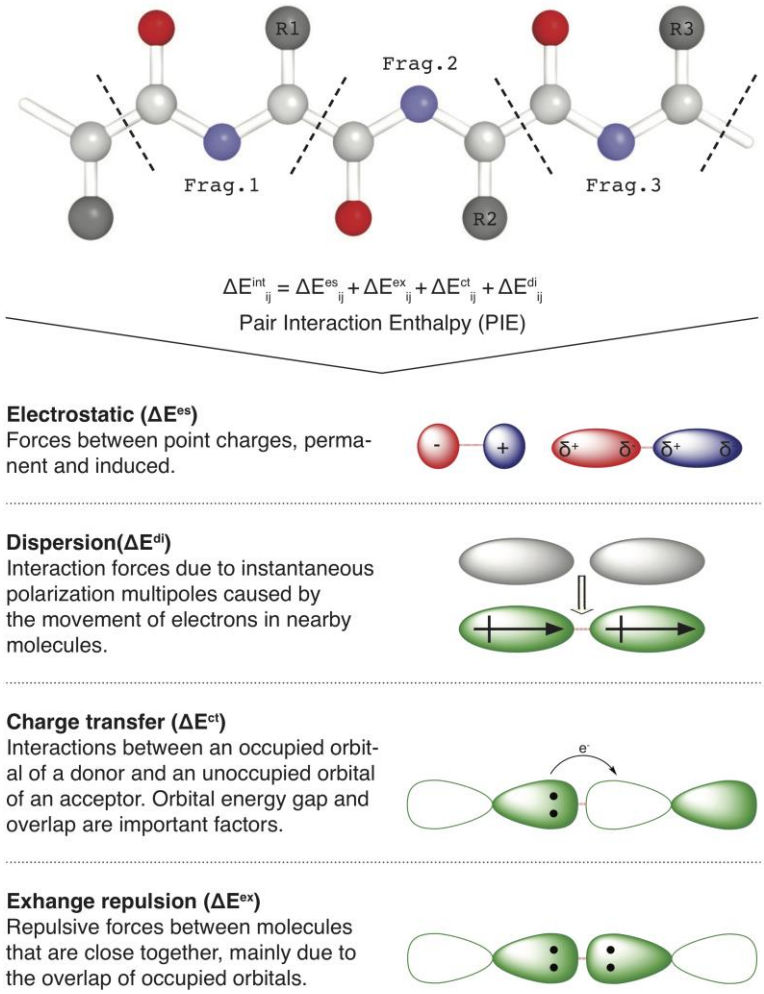


**Figure S1.** Workflow for PIEDA calculations and details on each of PIE terms that are computed. The electrostatic component arises from the Coulomb interaction between polarized charge distributions of fragments. The exchange repulsion term is derived from the interaction between fragments situated in proximity and is always repulsive; it is due to the Pauli repulsion and is related to the overlap of two occupied orbitals. The charge transfer term arises from the interaction between occupied orbitals of a donor and unoccupied orbitals of an acceptor. The dispersion arises as the interaction between instantaneous dipole moments of two fragments, it is hydrophobic (non-polar) in nature and is obtained in PIEDA from the correlation energy of electrons.

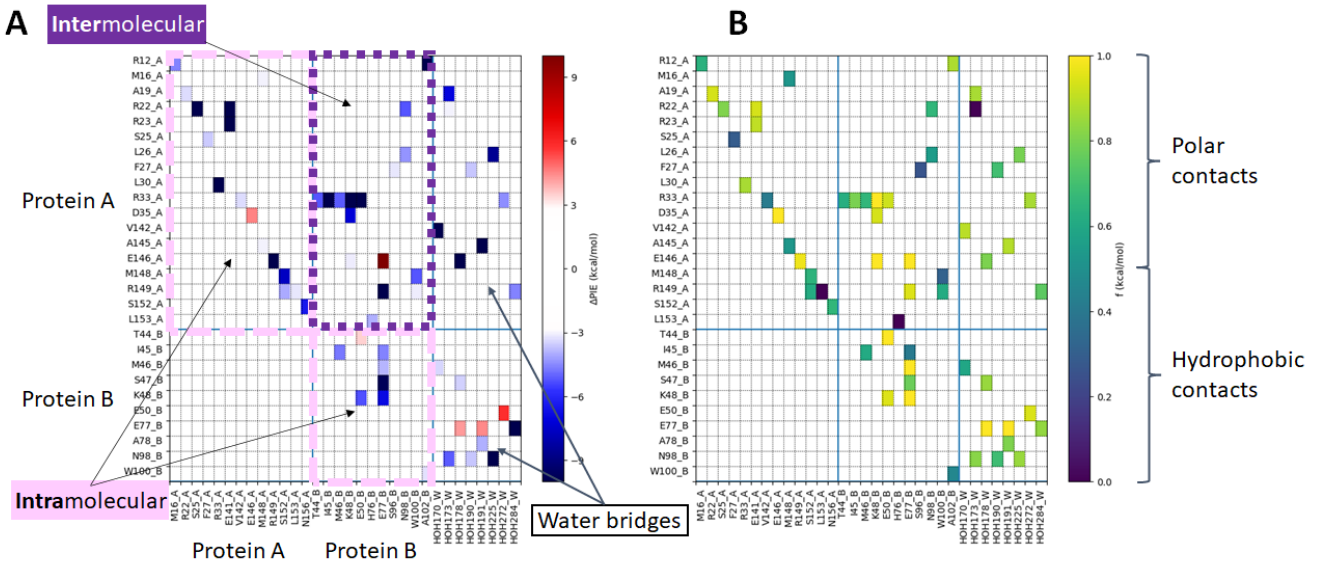


**Figure S2.** FMO-PPI results are displayed both in terms of ΔPIE (**A**) and chemical factor ***f*** (**B**). The top-left and bottom-middle sections (highlighted in pink) show intramolecular interactions between residues of protein A and protein B, respectively. Duplicate intermolecular interactions were removed leaving the bottom-left corner empty. The top-middle section (highlighted in purple) represents intermolecular interactions between residues within protein A and residues within protein B. The quadrants on the right side show the water bridges between residues of protein A and B. Color coding indicates the ΔPIE (**A**) and *f* (**B**) values for each interaction. The white boxes represent the absence of a contact.

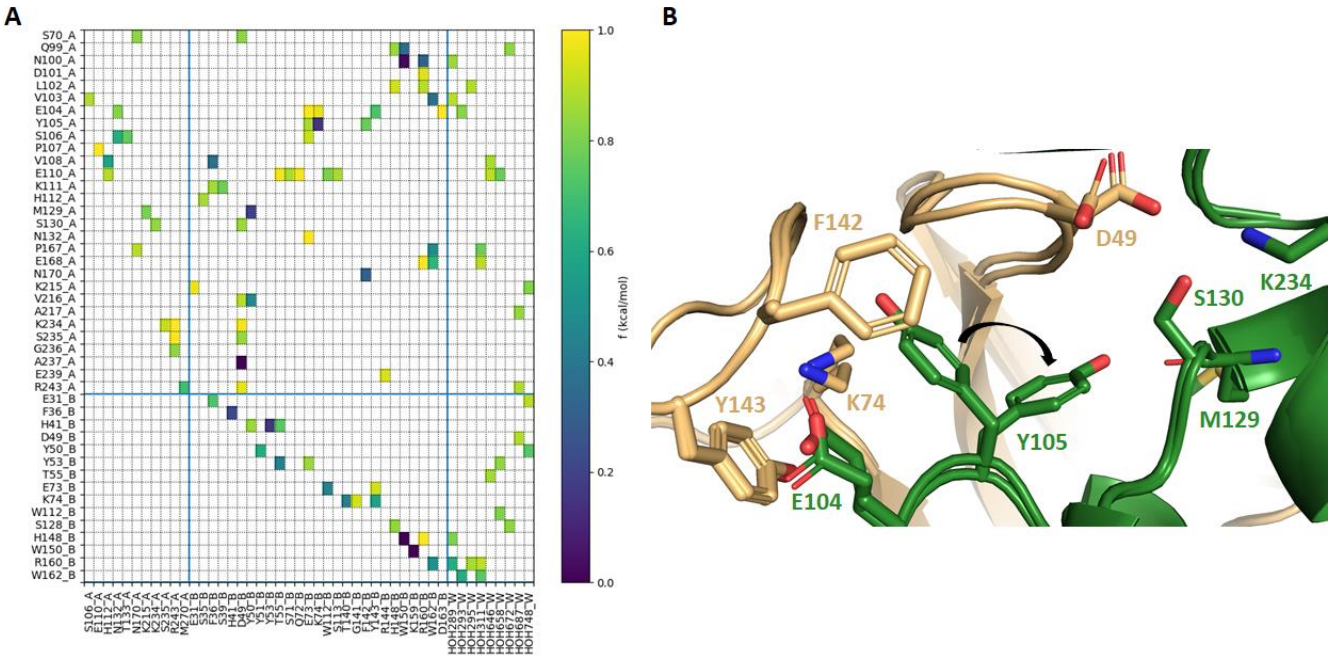


**Figure S3.** (**A**) the chemical character of the PPIs calculated with PIEDA for TEM1 in complex with BLIP. Heat map boxes are colored according to their ***f*** (chemical) factor: from dark blue (100% dispersion contribution) to yellow (100% electrostatic). The absence of a contact is represented by a white box. (**B**) TEM1 in complex with BLIP F142A (PDB code 1SoW) superposed with the WT complex (PDB code 1JTG). The conformation of Y105 dramatically changed upon F142 mutation into alanine (indicated by the black arrow). The white boxes represent the absence of a contact.

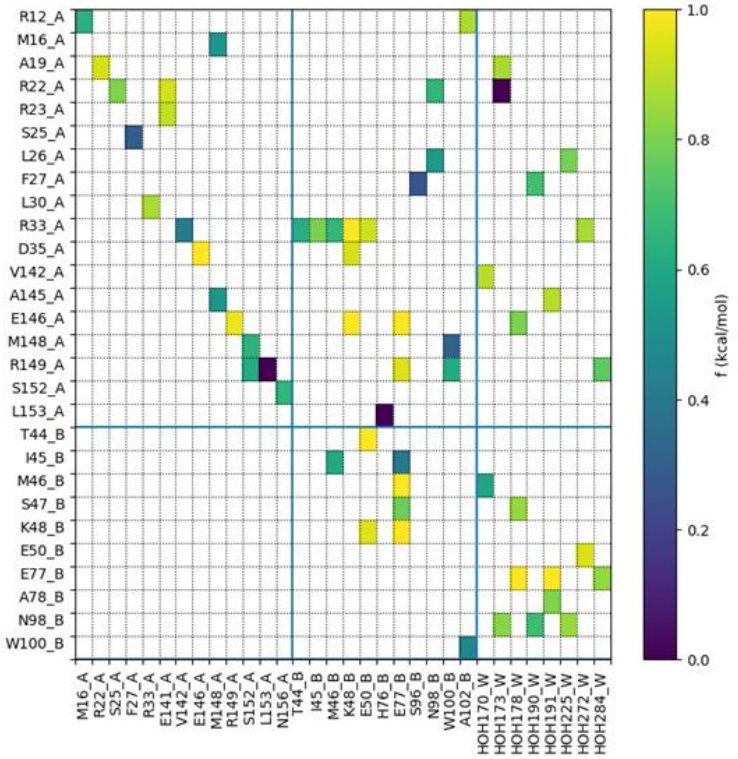


**Figure S4.** The chemical character of the PPIs calculated with PIEDA for IFNα2 in complex with IFNAR2. Heat map boxes are coloured according to their f (chemical) factor: from dark blue (100% dispersion contribution) to yellow (100% electrostatic). The white boxes represent the absence of a contact.

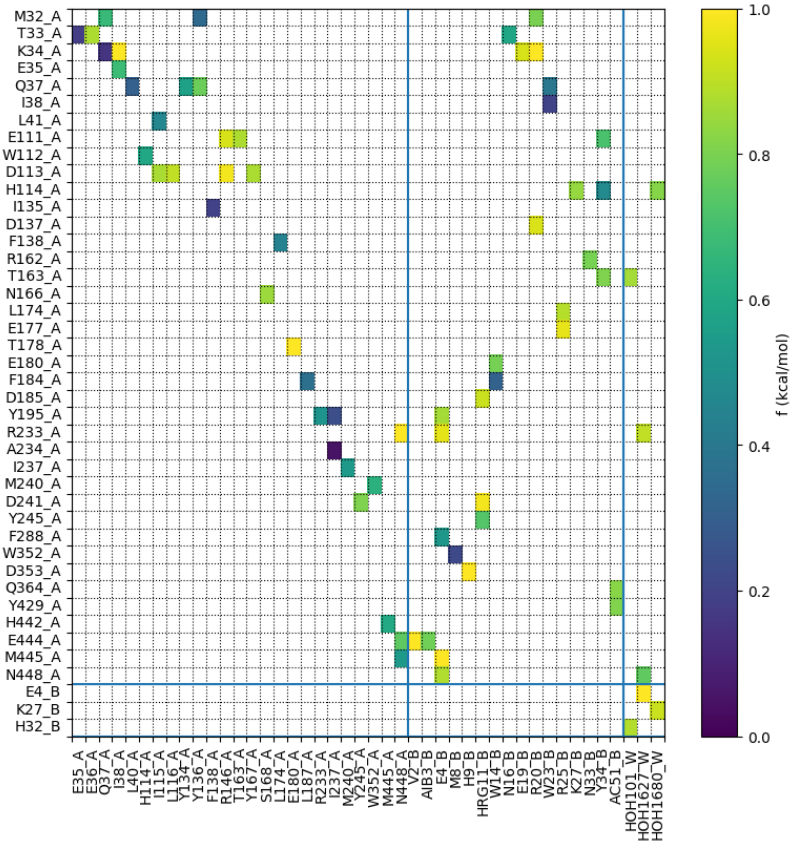


**Figure S5.** The chemical character of the PPIs calculated with PIEDA for PTH1R in complex with ePTH. Heat map boxes are coloured according to their f (chemical) factor: from dark blue (100% dispersion contribution) to yellow (100% electrostatic). The white boxes represent the absence of a contact.

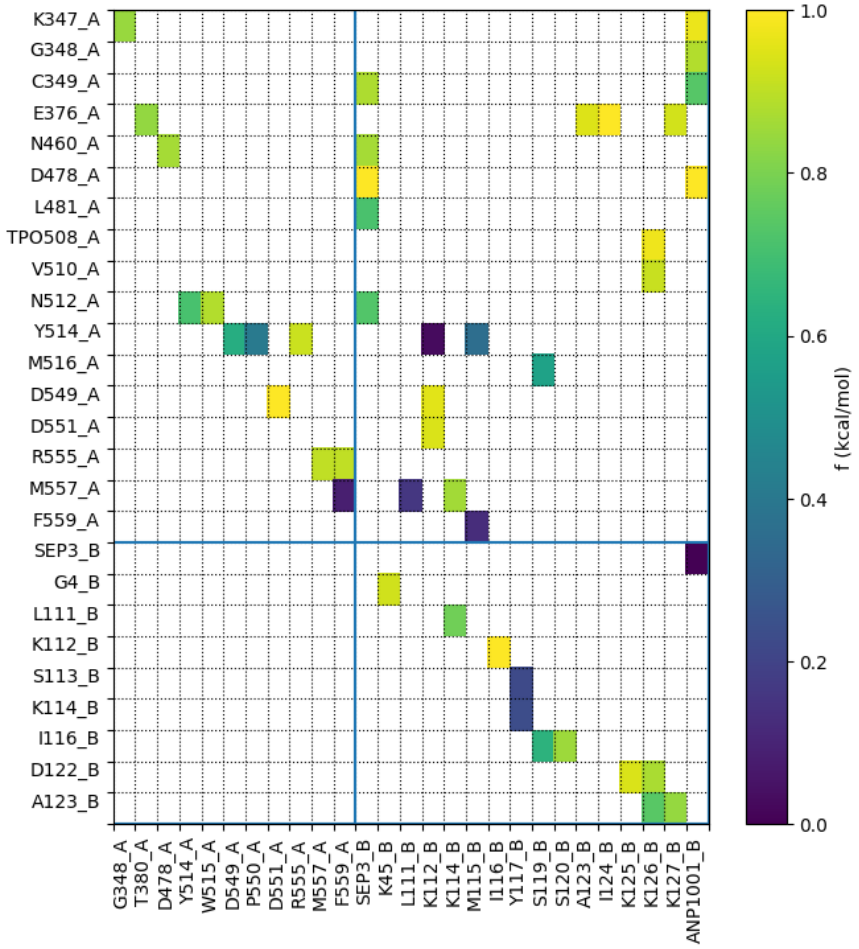


**Figure S6.** The chemical character of the PPIs calculated with PIEDA for LINK1 in complex with Cofilin-1. Heat map boxes are colored according to their f (chemical) factor: from dark blue (100% dispersion contribution) to yellow (100% electrostatic). The white boxes represent the absence of a contact.

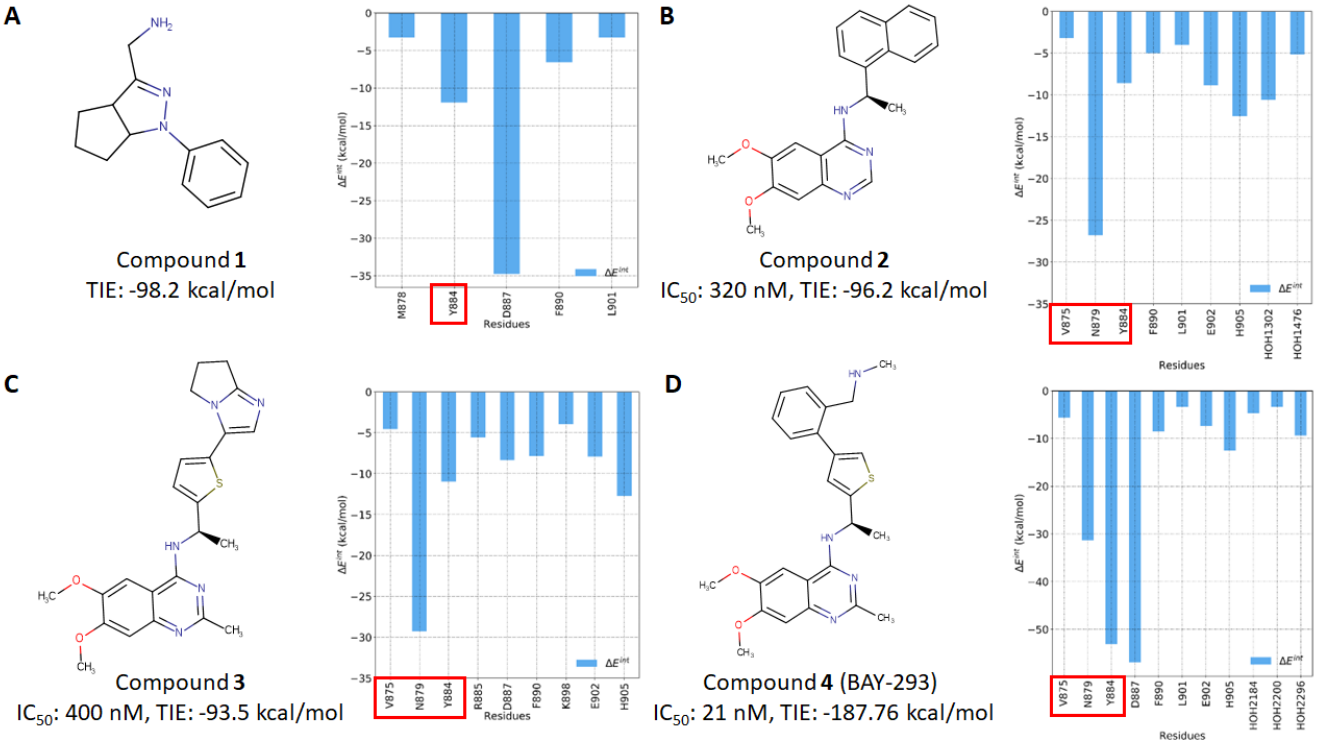


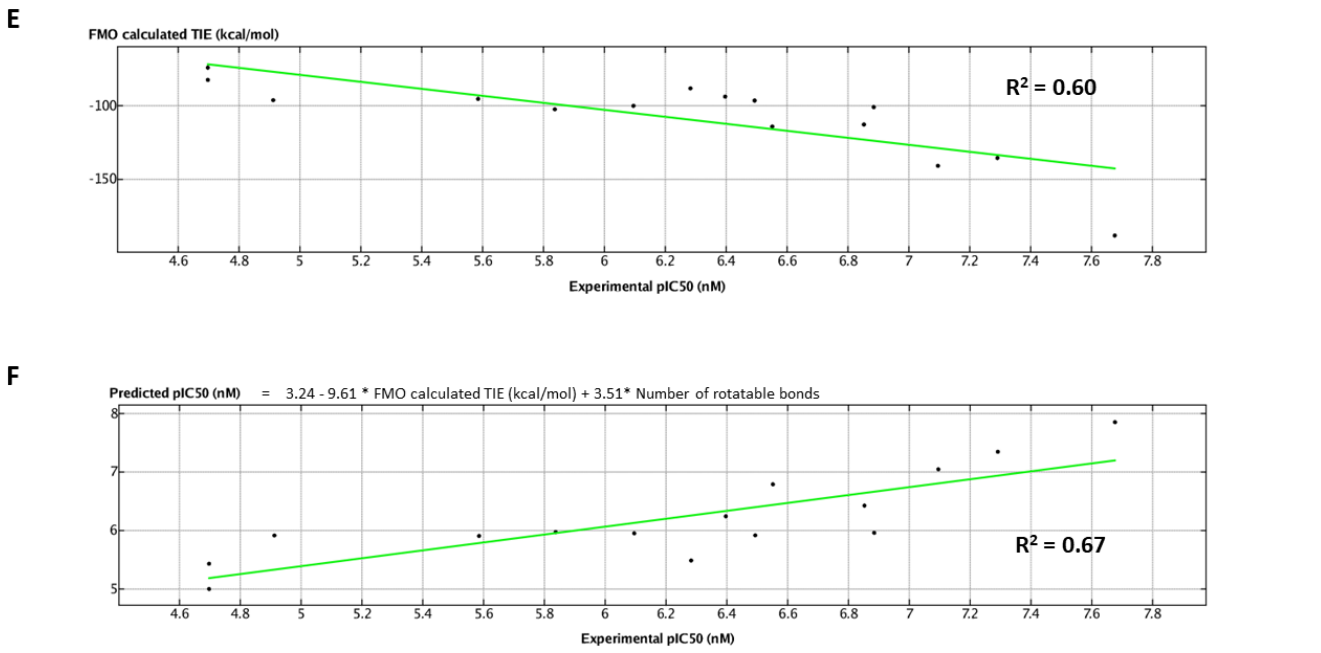


**Figure S7: (A-D)** 2D structures of SOS1 binders, experimental data extracted from literature, compared together with the TIE (total interaction energy) values that were calculated by FMO for each SOS1-ligand complex. The most significant residues are enclosed in red boxes. **(E)** Correlation plot between experimentally measured $pIC_{50}$ values[6] and calculated by FMO TIEs. **(F)** Correlation plot between experimentally measured[6] and predicted (FMO based) $pIC_{50}$ values.

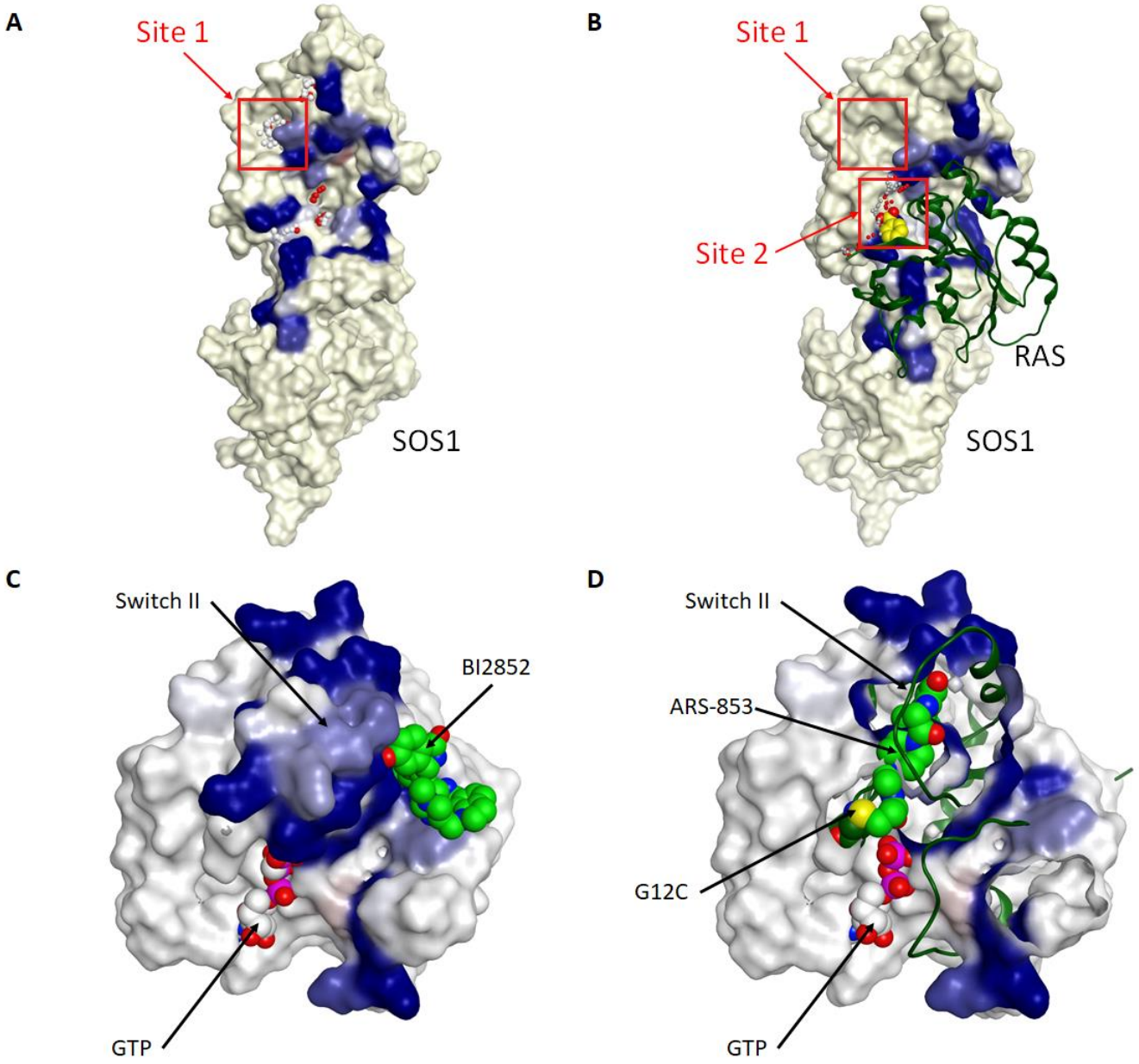


**Figure S8:** (**A**) To date, SOS1 inhibitors have been designed only for Site 1. (**B**) SOS1-RAS in complex with fragment binder in Site 2 (PDB 4URY) shows that molecular glues might be designed in a pocket between the two proteins, to stabilize the complex. (**C**) Crystal structure of KRAS G12D in complex with BI2852 (PDB 6GJ8), overlayed with the FMO-PPI results of SOS1-KRAS complex (PDB 6EPL). Carbon atoms of the ligand are coloured in green. (**D**) Crystal Structure of small molecule ARS-853 covalently bound to K-Ras G12C (PDB 5F2E), overlayed with the FMO-PPI results of SOS1-KRAS complex (PDB 6EPL). Surface of the Switch II loop is hidden. Carbon atoms of the ligand are coloured in green.

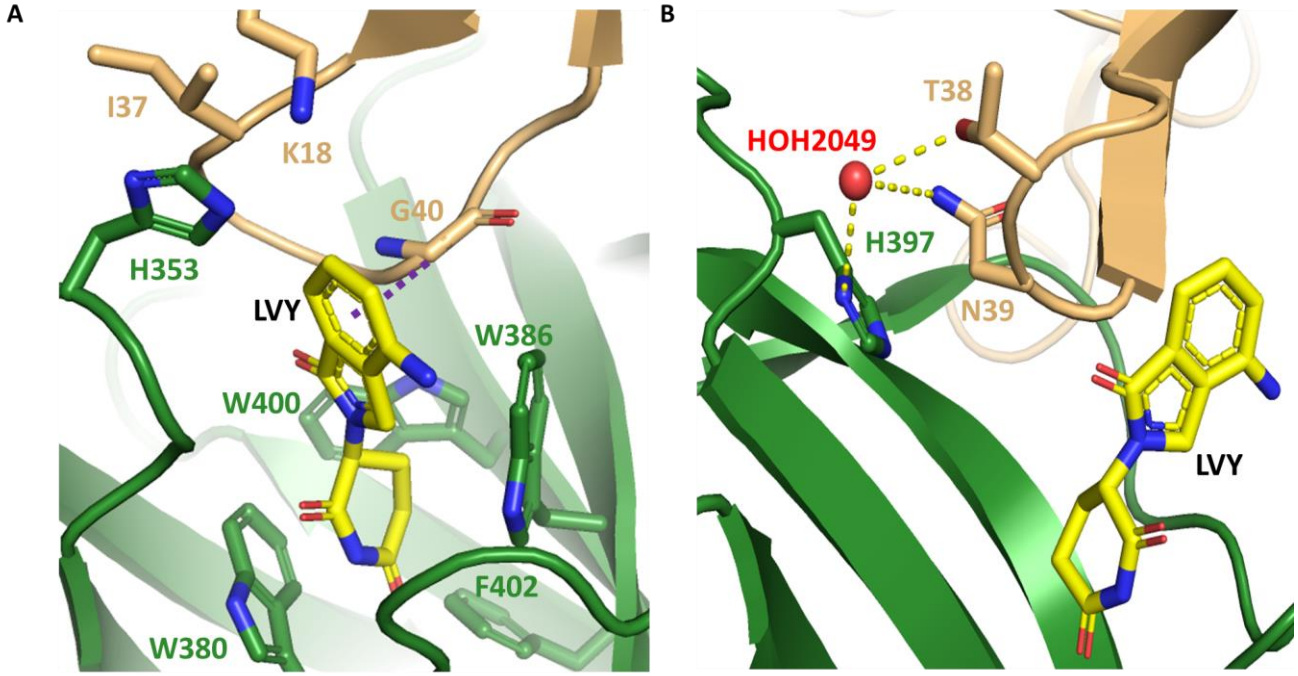


**Figure S9:** Crystal structure of CRBN-LVY-CK1α complex (PDB code 5FQD, CRBN and CK1α residues and ribbon coloured dark green and orange respectively, LVY carbons is coloured in light yellow). (**A**) Ligand binding pocket and key residues involved in LVY (yellow sticks) binding as detected by FMO. (**B**) Yellow dashed lines indicate water-bridges with 2049 HOH that stabilize the CRBN- CK1α complex.

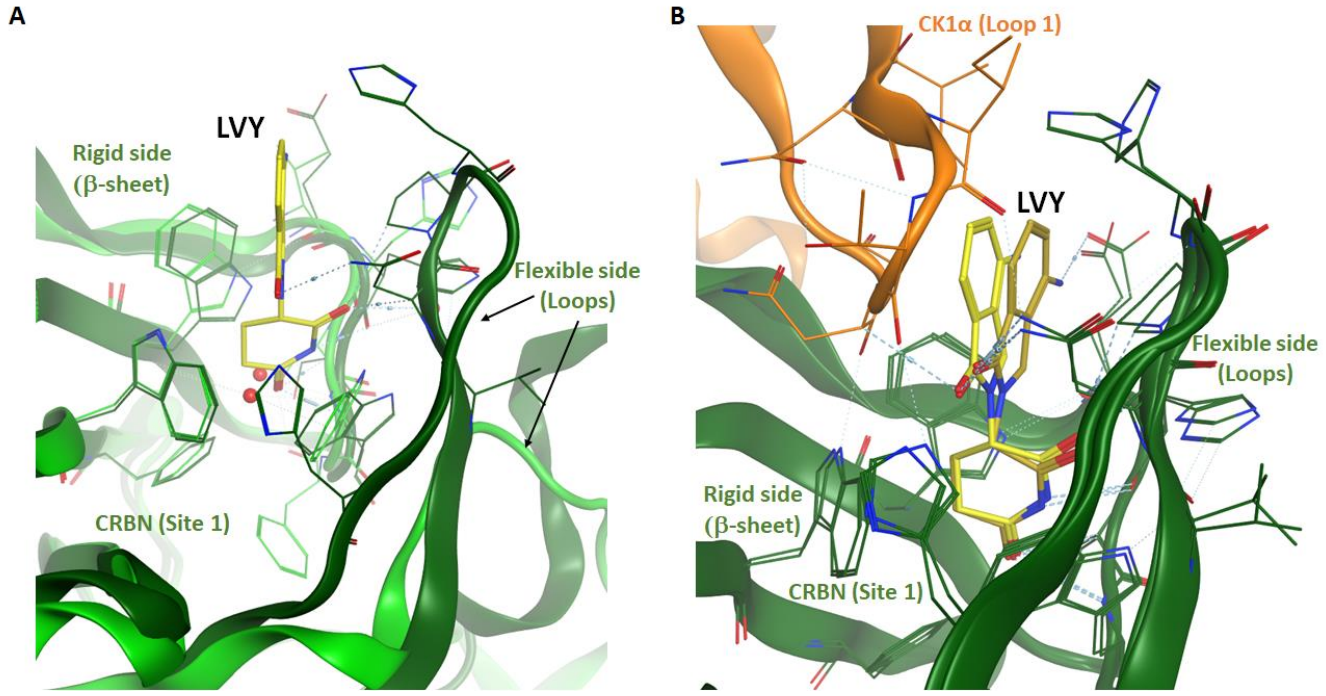


**Figure S10:** (**A**) Overlay/comparison of crystal structures of apo CRBN (PDB code 3WX2, CRBN residues and ribbon coloured light green) and CRBN-LVY complex (PDB code 4TZ4, CRBN residues and ribbon coloured dark green, LVY carbons is coloured in light yellow). LVY binding induces a structural change in the flexible side of CRBN, whereas the rigid side (on the left) did not change conformation. (**B**) Overlay/comparison of crystal structures of CRBN-LVY complex (PDB code 4TZ4, CRBN residues and ribbon coloured dark green, LVY carbons is coloured in light yellow) with CRBN-LVY-CK1α complex (PDB code 5FQD, CRBN and CK1α residues and ribbon coloured dark green and orange respectively, LVY carbons is coloured in light yellow). Binding of CK1α to CRBN-LVY complex does not affect the CRBN structure and cause light shift in the position of the phthalimide ring of LVY.

**Table S1:** Comparison of the effects of different mutations on the BLIP and TEM1 binding affinity[1, 2].

| Protein | Mutation | Protein-protein affinity* |
|---|---|---|
| BLIP | F36A | ↓↓ |
| | H41A | ↓↓ |
| | D49A | ↓ |
| | Y53A | ↓ |
| | S71A | ↓ |
| | K74A | ↓↓ |
| | W112A | ↓↓ |
| | S113A | -- |
| | F142A | ↓↓ |
| | Y143A | ↓ |
| | H148A | ↓↓ |
| | W150A | ↓↓ |
| | R160A | ↓ |
| | W162A | ↓ |
| TEM1 | Q99A | ↓ |
| | V103A | ↓ |
| | E104A | ↓↓ |
| | P107A | -- |
| | E110A | ↓↓ |
| | M129A | ↓ |
| | S130A | ↓ |
| | K234A | ↓ |
| | R243A | ↓↓ |

* ↓↓, large decrease in binding affinity (change in binding energy with respect to WT higher than 10 kJ/mol); ↓, statistically significant decrease in binding affinity (change in binding energy with respect to WT between 1 and 10 kJ/mol); --, no statistically significant decrease in binding affinity (change in binding energy with respect to WT less than 1 kJ/mol).

**Table S2:** Comparison of the effects of different mutations on the IFNα2 and IFNAR2 binding affinity[3].

| Protein | Mutation | Protein-protein affinity* |
|---|---|---|
| IFNα2 | R12A | ↓ |
| | L15A | ↓ |
| | M16A | -- |
| | R22A | ↓ |
| | L26A | ↓ |
| | F27A | ↓ |
| | L30A | ↓↓ |
| | R33A | ↓↓ |
| | H34A | ↓ |
| | D35A | ↓ |
| | A145G | ↓↓ |
| | M148A | ↓↓ |
| | R149A | ↓↓ |
| | S152A | ↓ |
| | L153A | ↓ |
| | N156A | -- |

* ↓↓, large decrease in binding affinity (Kd WT/Kd mutant ratio lower than 0.1); ↓, statistically significant decrease in binding affinity (Kd WT/Kd mutant ratio between 0.1 and 0.7); --, no statistically significant decrease in binding affinity (Kd WT/Kd mutant ratio higher than 0.7).

**Table S3:** Comparison of the effects of different mutations on the PTH1R and ePTH binding affinity[4].

| Protein | Mutation | Protein-protein affinity* |
|---|---|---|
| PTH1R | Y195A | ↓↓ |
| | L232A | -- |
| | R233A | ↓↓ |
| | V235A | -- |
| | L244A | ↓↓ |
| | F288A | ↓↓ |
| | W352A | ↓ |
| | M445E/A | ↓↓ |
| | N448D | ↓↓ |

* ↓↓, large decrease in binding affinity (ΔpIC50 with respect to WT lower than -1); ↓, statistically significant decrease in binding affinity (ΔpIC50 with respect to WT between -1 and -0.5); --, no statistically significant decrease in binding affinity (ΔpIC50 with respect to WT higher than -0.5).

**Table S4:** Comparison of the effects of different mutations on the LIMK1 and Cofilin-1 binding affinity[5].

| Protein | Mutation | Protein-protein binding* |
|---|---|---|
| Cofilin-1 | K112D | ↓↓ |
| Cofilin-1 | M115A | ↓↓ |
| Cofilin-1 | S119M | ↓↓ |
| LIMK1 | M516S | ↓↓ |
| LIMK1 | DDKK** | ↓↓ |

* ↓↓, large decrease in binding affinity (kinase assay signal of WT/signal of mutant higher than 5).

**DDKK: $D549K^{LIMK1}$ and $D551K^{LIMK1}$ double mutation.

**Table S5:** Total number of residues at the PPI interface for each protein-protein complex.

| System (Protein A – Protein B) | N. PPI residues at Protein A | N. PPI residues at Protein B |
|---|---|---|
| TEM1-BLIP | 44 | 46 |
| IFNα2-IFNAR2 | 32 | 29 |
| PTH1R-ePTH | 83 | 34 |
| LIMK1-Cofilin-1 | 37 | 27 |

REFERENCES

1. Reichmann, D.; Rahat, O.; Albeck, S.; Meged, R.; Dym, O.; Schreiber, G., The modular architecture of protein–protein binding interfaces. *Proceedings of the National Academy of Sciences of the United States of America* **2005**, 102, 57-62.
2. Reichmann, D.; Cohen, M.; Abramovich, R.; Dym, O.; Lim, D.; Strynadka, N. C. J.; Schreiber, G., Binding Hot Spots in the TEM1–BLIP Interface in Light of its Modular Architecture. *Journal of Molecular Biology* **2007**, 365, 663-679.
3. Thomas, C.; Moraga, I.; Levin, D.; Krutzik, Peter O.; Podoplelova, Y.; Trejo, A.; Lee, C.; Yarden, G.; Vleck, Susan E.; Glenn, Jeffrey S.; Nolan, Garry P.; Piehler, J.; Schreiber, G.; Garcia, K. C., Structural Linkage between Ligand Discrimination and Receptor Activation by Type I Interferons. *Cell* **2011**, 146, 621-632.
4. Ehrenmann, J.; Schöppe, J.; Klenk, C.; Rappas, M.; Kummer, L.; Doré, A. S.; Plückthun, A., High-resolution crystal structure of parathyroid hormone 1 receptor in complex with a peptide agonist. *Nature Structural & Molecular Biology* **2018**, 25, 1086-1092.
5. Hamill, S.; Lou, Hua J.; Turk, Benjamin E.; Boggon, Titus J., Structural Basis for Noncanonical Substrate Recognition of Cofilin/ADF Proteins by LIM Kinases. *Molecular Cell* **2016**, 62, 397-408.
6. Hillig, R. C.; Sautier, B.; Schroeder, J.; Moosmayer, D.; Hilpmann, A.; Stegmann, C. M.; Werbeck, N. D.; Briem, H.; Boemer, U.; Weiske, J.; Badock, V.; Mastouri, J.; Petersen, K.; Siemeister, G.; Kahmann, J. D.; Wegener, D.; Böhnke, N.; Eis, K.; Graham, K.; Wortmann, L.; von Nussbaum, F.; Bader, B., Discovery of potent SOS1 inhibitors that block RAS activation via disruption of the RAS–SOS1 interaction. *Proceedings of the National Academy of Sciences* **2019**, 116, 2551-2560.